



Dennis, R. J., Whitewoods, C. D., & Harrison, C. J. (2019). Quantitative methods in like for like comparative analyses of *Aphanoregma* (Physcomitrella) patens phyllid development. *Journal of Bryology*. <https://doi.org/10.1080/03736687.2019.1668109>

Peer reviewed version

Link to published version (if available):
[10.1080/03736687.2019.1668109](https://doi.org/10.1080/03736687.2019.1668109)

[Link to publication record in Explore Bristol Research](#)
PDF-document

This is the author accepted manuscript (AAM). The final published version (version of record) is available online via Maney Publishing at <https://www.tandfonline.com/doi/full/10.1080/03736687.2019.1668109> . Please refer to any applicable terms of use of the publisher.

University of Bristol - Explore Bristol Research

General rights

This document is made available in accordance with publisher policies. Please cite only the published version using the reference above. Full terms of use are available:
<http://www.bristol.ac.uk/red/research-policy/pure/user-guides/ebr-terms/>

1 **Quantitative methods in like for like comparative analyses of *Aphanoregma (Physcomitrella) patens***
2 **phyllid development.**

3 Ross J. Dennis^{1,2,3}, Chris D Whitewoods^{1,4}, and C. Jill Harrison^{1,5*}.

4 ¹ Department of Plant Sciences, University of Cambridge, Downing Street, Cambridge, CB2 3EA, UK.

5 ² Current address: Research School of Biology, The Australian National University, Canberra, ACT 2601,
6 Australia.

7 ³ Current address: Commonwealth Scientific and Industrial Research Organization (CSIRO), Canberra, ACT
8 2601, Australia.

9 ⁴ Current address: John Innes Centre, Norwich Research Park, Colney Lane, Norwich, NR4 7UH, UK

10 ⁵ Current address: School of Biological Sciences, University of Bristol, 24 Tyndall Avenue, Bristol, BS8 1TQ,
11 UK.

12 *Corresponding Author: Jill.Harrison@bristol.ac.uk.

13

14 **Word Count: 3295**

15

16

17

18

19

20

21

22 **Abstract**

23 *Physcomitrella patens* is an attractive model system for comparative analyses of leaf development because
24 it evolved leaves (phyllids) independently to flowering plants, yet its genome contains homologues of many
25 gene families that regulate angiosperm leaf development. In addition, *P. patens* phyllids are primarily a
26 single cell layer thick, making it simple to identify the cellular basis of defects that perturb shape.
27 Identification of gene functions in shape determination depends on like for like comparison of mutant
28 versus wild-type plants. Here we show that, if heteroblasty is not perturbed, such comparisons should use
29 phyllid L13 or above in the heteroblastic series, and fully expanded phyllids above P7 in the developmental
30 series. Using a quantitative approach, we show that heteroblastic size variation reflects differences in cell
31 proliferation rather than cell size and shape. A comparison of control to *pinA pinB* mutant phyllid
32 development verifies that PIN proteins promote cell proliferation and suppress expansion to determine
33 phyllid shape. The results and approach that we have generated will be applicable to any study of *P. patens*
34 phyllid development to reveal the cellular basis of phyllid size and shape variations.

35 **Key words**

36 *Aphanoregma*, *Physcomitrella*, phyllid, *pinA pinB*, leaf evolution, evo-devo.

37 **Main text**

38 **Introduction**

39 The plant evo-devo field aims to identify genes underpinning the radiation of diverse forms during
40 evolution (Harrison, 2017). Leaves and leaf-like organs have evolved multiple times and fulfil
41 photosynthetic functions during plant evolution (Tomescu, 2008; Harrison and Morris, 2018). Whilst the
42 leaves of vascular plants develop in the diploid sporophyte stage of the life cycle, the phyllids of mosses
43 and liverworts develop in the haploid gametophyte stage of the life cycle, and these groups evolved leaves
44 independently (Harrison and Morris, 2018). Moss phyllids each develop from a single cell cleft in a spiral
45 pattern from the gametophore apical cell (Parihar, 1967; Harrison *et al.*, 2009). The phyllid apical cell then
46 cleaves in a herringbone pattern thus establishing the proximo-distal and medio-lateral axes of phyllid
47 development, and later divisions extend both axes independently of the activity of the phyllid apical cell

48 (Harrison *et al.*, 2009). The resultant phyllid is oblanceolate, and except at the point of midrib insertion is a
49 single cell layer thick (Parihar, 1967; Harrison *et al.*, 2009). This property makes moss phyllids an attractive
50 model system for understanding how the activity of genes translates via cell growth and division into
51 overall organ form, particularly since it is possible to image all the cells within a phyllid as it grows (Harrison
52 *et al.*, 2009).

53 Reverse genetic approaches in *Aphanoregma patens* have started to identify genes that regulate phyllid
54 development in mosses to address questions about the genetic mechanisms underlying convergent leaf
55 evolution. Whilst some genetic mechanisms for leaf development are not shared between mosses and
56 flowering plants (e.g. (Sakakibara *et al.*, 2008)), many are. These include *TONNEAU* genes (Traas *et al.*,
57 1995) which regulate microtubule activity and phyllid expansion (Spinner *et al.*, 2010), *PIN* genes (Galweiler
58 *et al.*, 1998, Scarpella *et al.*, 2006) which regulate phyllid width (Bennett *et al.*, 2014; Viaene *et al.*, 2014)
59 and *HD-zipIII* genes (Talbert *et al.*, 1995; McConnell and Barton, 1998; Prigge *et al.*, 2005) which regulate
60 the proximodistal axis of phyllid development and phyllid margin integrity (Yip *et al.*, 2016). These genetic
61 data suggest that many similar mechanisms have been independently recruited to regulate leaf
62 development in mosses and flowering plants. Further *Aphanoregma* mutants such as *ftsZ* (Anja *et al.*, 2009)
63 and *RecQ* (Wiedemann *et al.*, 2018) have phyllids that are smaller than in wild-type plants or have split tips
64 respectively. Analyses of mutant phyllid phenotypes are to date qualitative and at the whole organ scale, so
65 do not reveal the cellular basis of mutant phenotypes. This makes it hard to draw comparisons between
66 wild-type and mutant plants or between studies (e.g. Spinner *et al.*, 2010, Bennett *et al.*, 2014, Viaene *et al.*,
67 2014, Yip *et al.*, 2016). Furthermore, *Aphanoregma* phyllids develop in a heteroblastic series (Barker
68 and Ashton, 2013) and different studies have intercepted this series at different points in development. For
69 these reasons, we have undertaken a quantitative analysis of phyllid development in *Aphanoregma* and
70 developed a simple approach to enable rigorous quantitative comparisons of phyllid phenotypes in wild-
71 type and mutant plants.

72 **Materials and Methods**

73 ***Plant growth and sample preparation***

74 The *Aphanoregma patens* Gransden strain was used in all experiments except for control versus mutant
75 phenotype comparisons, which used *pinA pinB* mutant strain and a *GH3::GUS* strain used to engineer the
76 *pinA pinB* mutants (Bierfreund *et al.*, 2003; Bennett *et al.*, 2014). All plants were grown as spot cultures on
77 BCDAT plates as described elsewhere (Whitewoods *et al.*, 2018). Phyllids were removed and laid out on
78 plates containing 0.8 % agar in heteroblastic series counting from the gametophore base. Phyllids L3, L10,
79 L14, L16, L18, and L20 were selected from each heteroblastic series and soaked in 1% chloral hydrate.
80 Cleared phyllids were rinsed with de-ionised water three times and transferred to 2 M NaOH for 2 h. They
81 were then rinsed and stained in toluidine blue prior to mounting under a coverslip with the abaxial side of
82 the phyllid lying flat against the slide (see supplementary protocol).

83 ***Microscopy, image capture and image segmentation***

84 Phyllids were imaged using a Leica DMRXA microscope with a 20 x objective. Length measurements were
85 made from the tip to the base along the midrib, and width measurements were made perpendicular to the
86 midrib at the widest point of each phyllid. Images were further processed with ImageJ (Schindelin, *et al.*,
87 2012) to generate a map of all cell outlines within the phyllid, and the length, width, area and aspect
88 (length to width) ratio of all cells was measured using ImageJ (see supplementary protocol). Using QGIS
89 software (QGIS Development Team, 2017), these metrics were plotted back against cell maps of each
90 phyllid to visualise cell shape trends within and between phyllids as heat maps.

91 **Results**

92 ***Heteroblastic variation in phyllid length reflects cell division, not expansion***

93 To quantify patterns of phyllid development, the five largest gametophores were teased out from five
94 different 6 week-old plants (n = 25 in total). Phyllids were removed from each gametophore, arranged in a
95 heteroblastic series and measured as described in the Materials and Methods section. Length
96 measurements were found to progressively increase to a maximum at phyllid L13 (Figure 1A), and thus
97 subsequent fully expanded phyllids in the heteroblastic series had a similar length (Figure 1A, Table S1).
98 However, phyllid length decreased towards the gametophore apex from P7 to P1 due to incomplete

99 expansion (Figure 1B, Table S2). To investigate the effect of cell size and shape on phyllid size, we mapped
100 the outline of cells in fully expanded phyllids throughout the heteroblastic series (Figure 1C). Quantitative
101 analyses of cell number per phyllid, cell length, cell width, cell area and cell aspect ratio supported previous
102 analyses showing that the increase in phyllid length in a heteroblastic series reflects an increase in cell
103 number rather than cell length increases (Figure 1D-H, Table S3).

104 ***Cell shapes are heterogeneously distributed***

105 To identify the cellular basis of differences in phyllid size and shape, we first plotted the distribution of
106 quantitative cell shape measures against phyllid cell maps using QGIS software (Figure 2A-D). This analysis
107 revealed a proximo-distal gradient in cell length, with high cell lengths in cells at the base and margin
108 (Figure 2A). There was a decrease in cell width from the base of the phyllid to the tip, but marginal cells
109 were the narrowest (Figure 2B). Cell area decreased from the base to the tip of phyllids (Figure 2C). In
110 contrast, cell aspect ratio increased from the midrib to the edge of the phyllid, with a slight decrease
111 towards the tip (Figure 2D). Thus, cells in different regions of *P. patens* phyllids had different quantitative
112 attributes.

113 ***Multivariate analysis distinguishes three phyllid regions with distinct cell shapes***

114 To determine whether the quantitative measures above were sufficient to distinguish phyllid regions with
115 different cellular identities, we performed a multivariate analysis using K means cluster analysis (Figure 3).
116 This identified three highly supported cell shape classes in all samples (Figure 3A and 3B, Table S4). The
117 spatial distribution of shape classes was plotted against phyllid cell maps using QGIS software. Whereas
118 cells at the base of the phyllid were long and broad, cells at the edge were long and narrow, and cells at the
119 top were shorter and narrower than cells at the base (Figure 3B, 3C). There was no difference in the cell
120 shape distribution or the proportions of each cell type between phyllids within a heteroblastic series. Thus
121 heteroblasty reflects differences in cell number, not cell shape and size.

122 ***Comparison of control with mutant phyllid phenotypes***

123 *Aphanoregma pinA pinB* mutants have defective auxin transport and previously identified phyllid defects
124 (Bennett *et al.*, 2014; Viaene *et al.*, 2014). To determine whether a quantitative approach would be useful
125 in mutant phenotype characterisation, we compared *pinA pinB* mutant development to development in a
126 *GH3::GUS* line used to engineer the *pinA pinB* mutant (Bierfreund *et al.*, 2003; Bennett *et al.*, 2014). To
127 identify any heteroblasty defects in mutants, we first measured phyllid lengths (Figure 4A, Table S5). Whilst
128 *pinA pinB* phyllids were longer than *GH3::GUS* phyllids, both lines reached a maximum length by phyllid L13
129 in the heteroblastic series (Figure 4A, 4B). Further analyses between genotypes compared the number of
130 cells and mean cell length, width, area and aspect ratio in fully expanded phyllids. This revealed that *pinA*
131 *pinB* mutants have fewer cells per phyllid than *GH3::GUS* plants, and that cells are longer and larger with a
132 similar width in mutant versus *GH3::GUS* plants (Figure 4C, Table S6).

133 To investigate the effect of genotype on cell shape, size and number in different phyllid regions we applied
134 the multivariate analysis and clustering approach described above to data from mutant and control
135 phyllids. This showed fewer cells in the top phyllid region in *pinA pinB* mutants compared to *GH3::GUS*
136 plants and slightly more cells in the edge region (Figure 4D, 4E). The base region had comparable cell
137 numbers. While there was no significant overall difference in cell area, cells in *pinA pinB* mutant phyllids
138 were slightly but significantly longer than cells in *GH3::GUS* lines (Figure 4D, Table S7). Comparison of
139 phyllid regions showed that cells from the edge and top regions in *pinA pinB* mutants were slightly larger
140 than equivalent cells in *GH3::GUS* plants (Figure 4D), and *pinA pinB* mutants had significantly wider cells in
141 the edge region and narrower cells in the top region with correspondingly altered aspect ratios. Cells in the
142 base region were unchanged in both width and aspect ratio in *pinA pinB* mutants compared to *GH3::GUS*
143 plants. The differences above were clear from heat maps plotting quantitative data and the output from
144 cluster analyses (Figure 4E). These data suggest that phyllid size and shape differences in *pinA pinB* mutants
145 are due to a small global increase in cell size and a reduction in the number of cells in the top phyllid region
146 (Figure 4E).

147 Discussion

148 The data above show that simple quantitative measures can be used to highlight the cellular basis of

149 differences in phyllid shape and size between control and mutant *P. patens* plants. A previous analysis of
150 phyllid development documented an increase in length through the heteroblastic series and increasing cell
151 number per phyllid correlating with progression through the heteroblastic series up to L10 (Barker and
152 Ashton, 2013). By further sampling we found that phyllid length and cell number per half phyllid reach a
153 maximum by phyllid L13 in the heteroblastic series. Our analyses also show that, regardless of size or
154 position in the heteroblastic series, phyllids contain three quantitatively distinct populations of cells.
155 Differences in phyllid size and shape reflect cell proliferation rather than cell expansion and cell shape
156 change. Thus, future studies wishing to draw like for like comparisons of phyllid development should rule
157 out heteroblastic defects and select phyllids L13 or above from the heteroblastic series and P8 or above
158 from the developmental series, and the quantitative approach that we have developed may be helpful in
159 characterising the cellular basis of mutant phenotypes.

160 Previous analyses have shown that the plant hormones cytokinin and auxin regulate phyllid size. Whilst
161 cytokinin promotes medio-lateral and proximo-distal proliferation, auxin suppresses medio-lateral and
162 proximo-distal proliferation and promotes anisotropic growth (Barker and Ashton, 2013). *pinA pinB*
163 mutants show similar phyllid phenotypes to normal plants treated with exogenous auxins (Bennett *et al.*,
164 2014; Viaene *et al.*, 2014), suggesting that PIN function is normally required to drain auxin from the phyllid
165 and confer phyllid shape by regulating the interplay between cell proliferation and growth. Here we have
166 refined this analysis to show that *pinA pinB* mutant phyllids have fewer cells in the top region, suggesting
167 that the role of PIN and auxin for cell proliferation may be localised, whereas its role in regulating cell
168 expansion is broader. The combination of simple hormonal inputs with the ability to understand
169 development at the gene, cell and organ scales makes the *P. patens* phyllid an attractive model system for
170 future analyses of mechanisms underlying organ shape determination in plants.

171 **Acknowledgements:**

172 We thank The Gatsby Charitable Foundation (GAT2962), The Royal Society (UF130563) and BBSRC
173 (BB/L00224811) for funding our work. We thank Zoe Nemec Venza for testing the segmentation protocol.

174 **Declaration of interest:**

175 We have no competing financial interests.

176 **References:**

- 177 **Martin A., Lang D., Hanke S.T., Mueller S.J., Sarnighausen E., Vervliet-Scheebaum M. and Reski, R., 2009.**
178 Targeted gene knockouts reveal overlapping functions of the five *Physcomitrella patens* FtsZ isoforms in
179 chloroplast division, chloroplast shaping, cell patterning, plant development, and gravity sensing. *Molecular*
180 *plant* 2: 1359-1372.
- 181 **Barker E.I. and Ashton N.W. 2013.** Heteroblasty in the moss, *Aphanoregma patens* (*Physcomitrella patens*),
182 results from progressive modulation of a single fundamental leaf developmental programme. *Journal of*
183 *Bryology* 35: 185-196.
- 184 **Bennett T.A., Liu M.M., Aoyama T., Bierfreund N.M., Braun M., Coudert Y., Dennis R.J., O'Connor D.,**
185 **Wang X.Y., White C.D., Decker E.L., Reski R. and Harrison C.J. 2014.** Plasma membrane-targeted PIN
186 proteins drive shoot development in a moss. *Current Biology* 24: 2776-2785.
- 187 **Bierfreund N.M., Reski, R., Decker, E.L. 2003.** Use of an inducible reporter gene system for the analysis of
188 auxin distribution in the moss *Physcomitrella patens*. *Plant Cell Reports* 21: 1143-1152.
- 189 **Galweiler L., Guan C., Muller A., Wisman E., Mendgen K., Yephremov A. and Palme K. 1998.** Regulation of
190 polar auxin transport by AtPIN1 in *Arabidopsis* vascular tissue. *Science* 282: 2226-2230.
- 191 **Harrison C.J., Roeder A.H.K., Meyerowitz E.M. and Langdale J.A. 2009.** Local cues and asymmetric cell
192 divisions underpin body plan transitions in the moss *Physcomitrella patens*. *Current Biology* 19: 461-471.
- 193 **Harrison C.J. 2017.** Development and genetics in the evolution of land plant body plans. *Philosophical*
194 *Transactions of the Royal Society B* 372: e20150490.
- 195 **Harrison C.J. and Morris J.L. 2018.** The origin and early evolution of vascular plant shoots and leaves.
196 *Philosophical Transactions of the Royal Society B* 373: e20160496.
- 197 **McConnell J.R. and Barton M.K. 1998.** Leaf polarity and meristem formation in *Arabidopsis*. *Development*
198 125: 2935-2942.
- 199 **Parihar N.S. 1967.** *Bryophyta* (5th edition). Allahabad: Indian Universities Press.

200 **Prigge M.J., Otsuga D., Alonso J.M., Ecker J.R., Drews G.N. and Clark S.E. 2005.** Class III homeodomain-
 201 leucine zipper gene family members have overlapping, antagonistic, and distinct roles in *Arabidopsis*
 202 development. *The Plant Cell* 17: 61-76.

203 **QGIS Development Team 2017.** QGIS Geographic Information System. Open Source Geospatial Foundation
 204 Project. <http://www.qgis.org/>

205 **Sakakibara K., Nishiyama T., Deguchi H., Hasebe M. 2008.** Class 1 *KNOX* genes are not involved in shoot
 206 development in the moss *Physcomitrella patens* but do function in sporophyte development. *Evolution and*
 207 *Development* 10: 555-66.

208 **Scarpella E., Marcos D., Friml J. and Berleth T. 2006.** Control of leaf vascular patterning by polar auxin
 209 transport. *Genes and Development* 20: 1015-1027.

210 **Schindelin, J.; Arganda-Carreras, I. & Frise, E. et al. 2012.** Fiji: an open-source platform for biological-image
 211 analysis. *Nature methods* 9: 676-682

212 **Spinner L., Pastuglia M., Belcram K., Pegoraro M., Goussot M., Bouchez D. and Schaefer D.G. 2010.** The
 213 function of TONNEAU1 in moss reveals ancient mechanisms of division plane specification and cell
 214 elongation in land plants. *Development* 137: 2733-2742.

215 **Talbert P.B., Adler H.T., Parks D.W. and Comai L. 1995.** The *REVOLUTA* gene is necessary for apical
 216 meristem development and for limiting cell divisions in the leaves and stems of *Arabidopsis thaliana*.
 217 *Development* 121: 2723-2735.

218 **Tomescu, A.M.F. 2008.** Megaphylls, microphylls and the evolution of leaf development. *Trends in Plant*
 219 *Science* 14: 5-12.

220 **Traas, J., Bellini, C., Nacry, P., Kronenberger, J., Bouchez, D., and Caboche, M. 1995.** Normal
 221 differentiation patterns in plants lacking microtubular preprophase bands. *Nature* 375: 676-677.

222 **Viaene, T., Landberg, K., Thelander, M., Medvecka, E., Pederson, E., Feraru, E., Cooper, E.D., Karimi, M.,**
 223 **Delwiche, C.F., Ljung, K., et al. 2014.** Directional auxin transport mechanisms in early diverging land plants.
 224 *Current Biology* 24: 2786-2791.

225 **Whitewoods, C.D., Cammarata, J., Venza, Z.N., Sang, S., Crook, A.D., Aoyama, T., Wang, X.Y., Waller, M.,**
226 **Kamisugi, Y., and Cuming, A.C. 2018.** *CLAVATA* was a genetic novelty for the morphological innovation of
227 3D growth in land plants. *Current Biology* 28: 2365-2376.

228 **Wiedemann G., van Gessel N., Köchl F., Hunn L., Schulze K., Maloukh L., Nogué F.,**
229 **Decker E.L., Hartung F. and Reski R., 2018.** RecQ helicases function in development, DNA
230 repair, and gene targeting in *Physcomitrella patens*. *The Plant Cell* 30: 717-736.

231 **Yip, H.K., Floyd, S.K., Sakakibara, K., and Bowman, J.L. 2016.** Class III *HD-Zip* activity
232 coordinates leaf development in *Physcomitrella patens*. *Developmental Biology* 419: 184-197.

233
234

Figure and figure captions

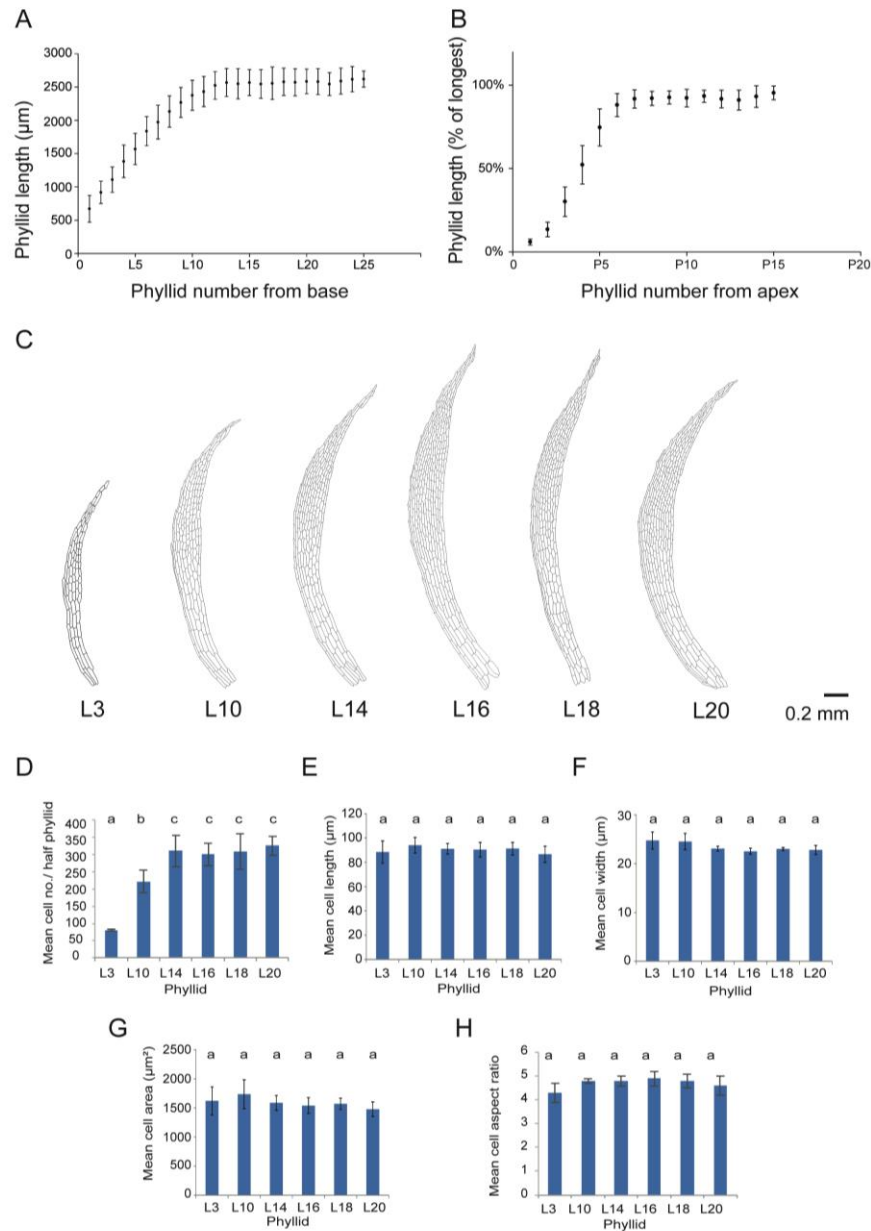
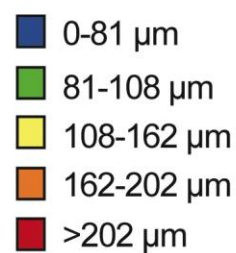
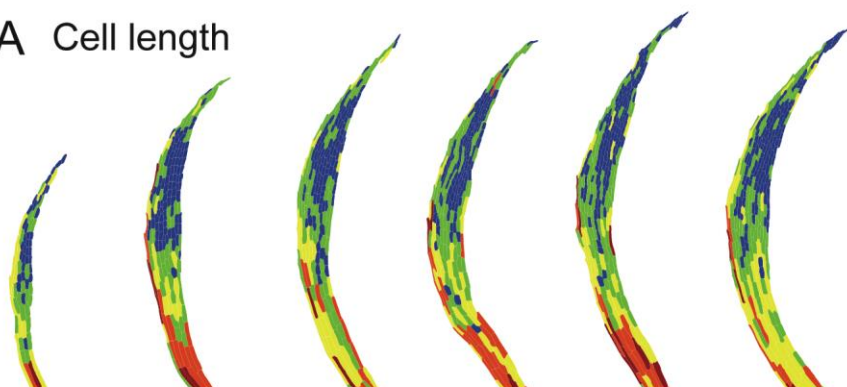
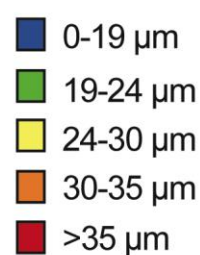
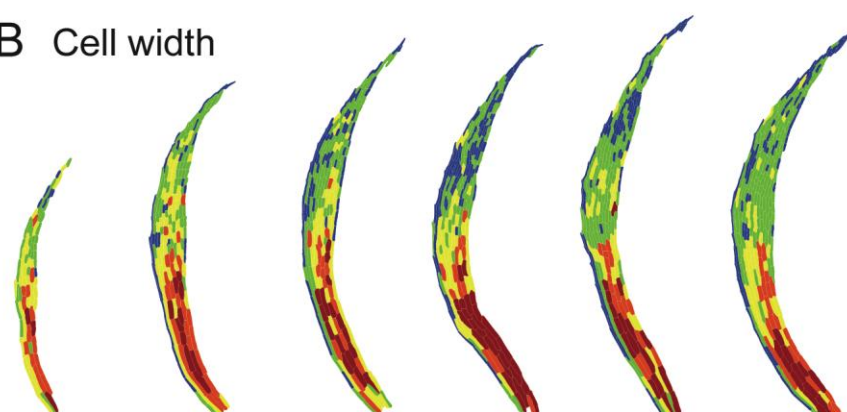


Figure 1: Heteroblasty reflects differences in cell number in *P. patens*, and phyllid length reaches a maximum by L13. (A) The mean length of phyllids in heteroblastic series. (B) The length as a proportion of the maximum of phyllids in developmental series. (C) Cell outlines segmented from representative phyllids in a heteroblastic series, with the position in series denoted. Scale bar = 0.2 mm. (D-H) Quantitative analyses of half phyllid cell numbers (D), cell length (E), cell width (F), cell area (G) and cell aspect ratio (H) showed that phyllid length varied in proportion to cell number. Error bars represent standard deviation and differences supported by ANOVA with p values ≤ 0.05 are noted above graphs.

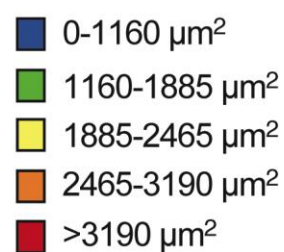
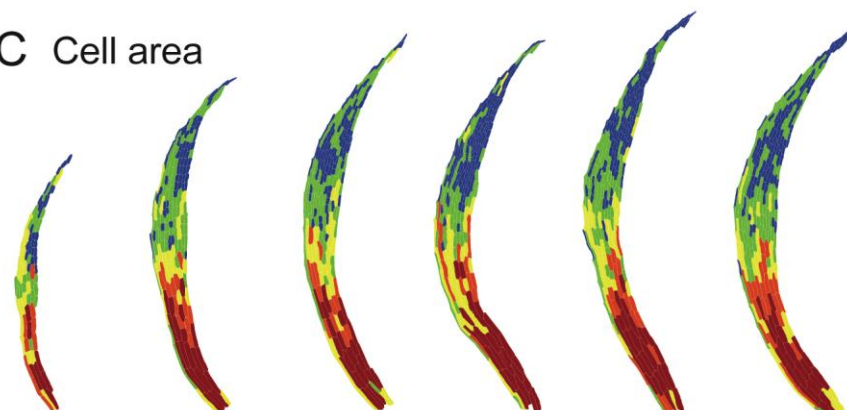
A Cell length



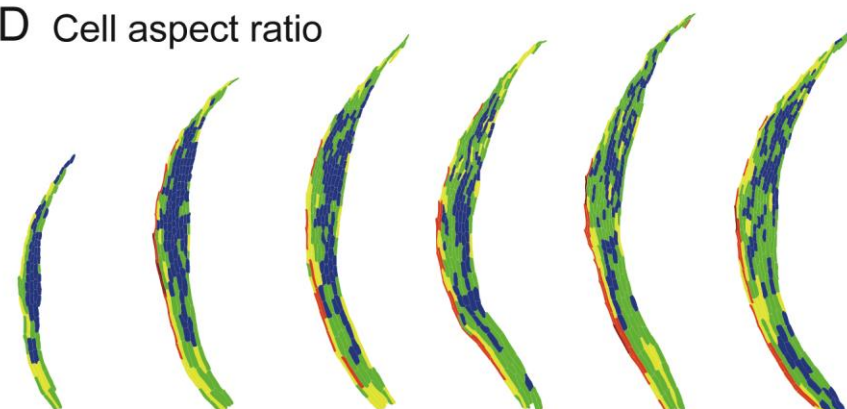
B Cell width



C Cell area



D Cell aspect ratio



L3

L10

L14

L16

L18

L20

0.2 mm

258 **Figure 2: Regional cell shape and size variation in *P. patens* phyllids.** (A-D) Heat maps showing distribution
 259 of phyllid cell lengths (A), widths (B), areas (C) and aspect ratios (D) calculated for phyllids L3, L10, L14, L16,
 260 L18

261 and

262 L20

263 in a

264 heter

265 oblas

266 tic

267 serie

268 s.

269 Scale

270 bar =

271 0.2

272 mm.

273

274

275

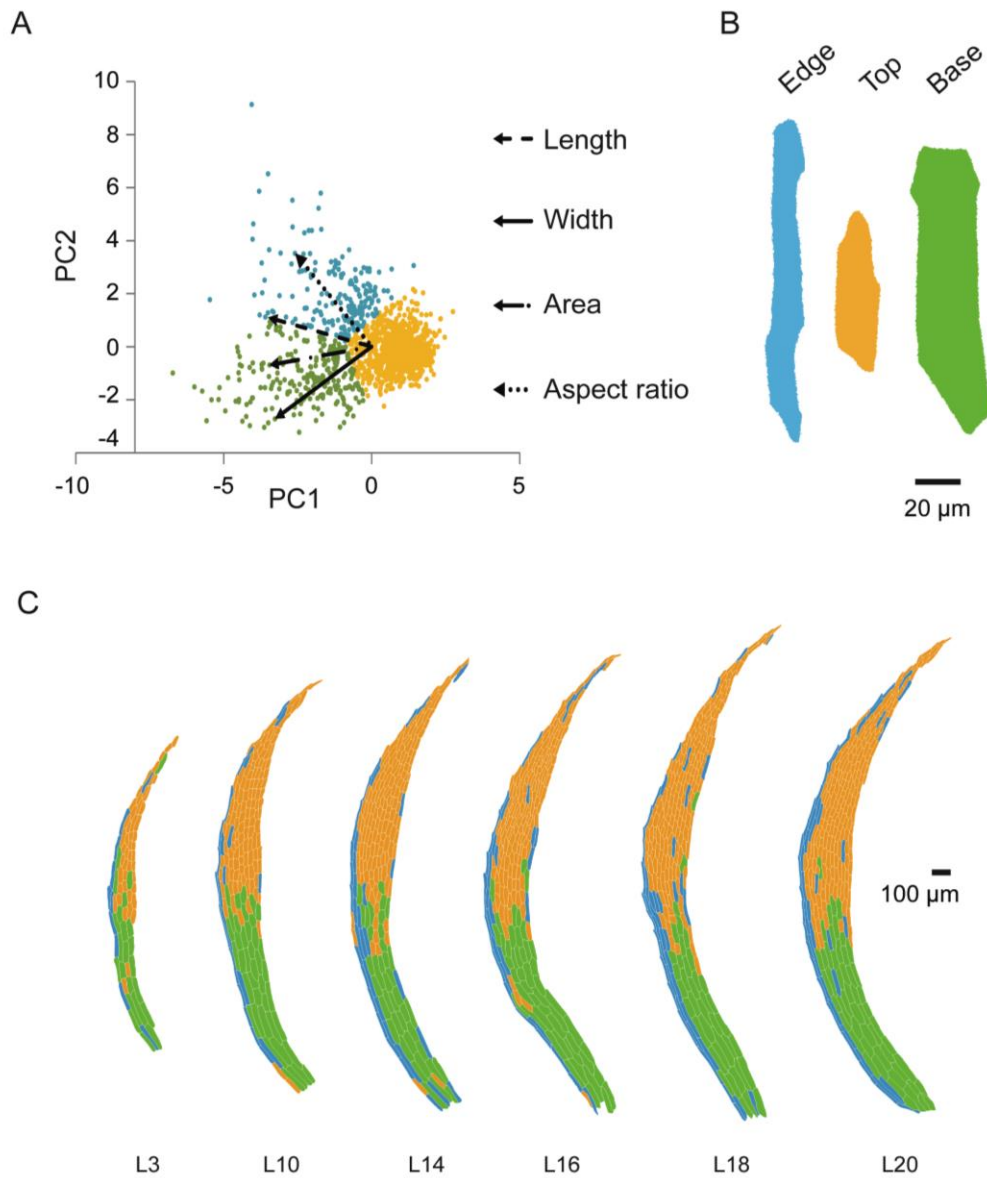
276

277

278

279

280



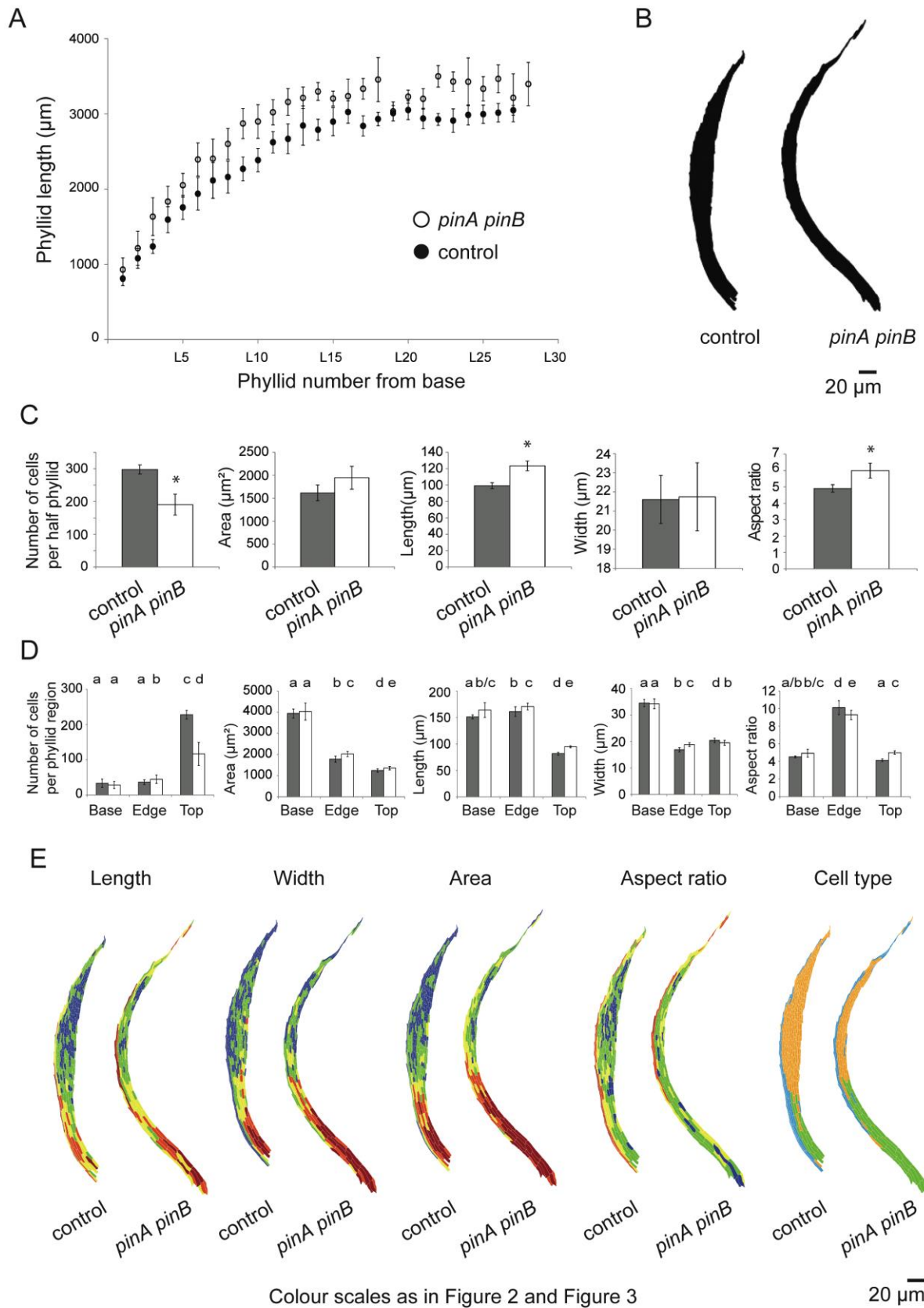
281

282

283

284

285 **Figure 3: Multivariate analysis identified three phyllid regions with distinct cell shapes.** A) Multivariate
286 analysis distinguished three groups of cells on the basis of length, width, area and aspect ratio. Arrows
287 illustrate the effect of changes in each variable. B) Cells with elongated (edge), small (top) or larger (base)
288 shapes representing each cluster were identified. Scale bar = 20 μm . C) Cell maps of phyllids L3, L10, L14,
289 L16, L18, L20 showing the distribution of edge, top and base cells. Scale bar = 100 μm .



290

291 **Figure 4: Quantitative comparison of *pinA pinB* to control phyllid phenotypes.** (A) Graph showing
 292 heteroblastic length changes of *GH3::GUS* and *pinA pinB* mutant phyllids. Error bars represent standard

293 deviation (B) Silhouettes showing differences in shape between wild-type and *pinA pinB* mutant phyllids.
294 Scale bar = 20 μm . (C) Cell metrics of wild-type and mutant phyllids calculated from phyllid L16-L20 in the
295 heteroblastic series. * indicates significant differences in t-test with p values ≤ 0.05 . (D) Output of
296 multivariate analysis showing that *pinA pinB* mutant phyllids differ from wild-type phyllids in the number of
297 cells in the 'top' region of the phyllid. Cells in each region were identified by their shape attributes, and as
298 expected no differences in area, length, width or aspect ratio were detected. Error bars represent standard
299 deviation. Differences supported by ANOVA with p values ≤ 0.05 are noted above graphs. (E) Distribution of
300 cellular attributes in wild-type and *pinA pinB* mutant phyllids. Colour scales as in Figure 2 and Figure 3.
301 Scale bar = 20 μm .

302

303 Supplementary data

304 Table S1

305

306

307

308

309

310

311

312

313

314

315

316

317

318

319

320

321

322

323 Table S2

324

325

326

327

328

329

330

331

332

Table S1: The length of phyllids at different positions in heteroblastic series	
Phyllid position in heteroblastic series	Mean phyllid length in μm \pm standard deviation (n = 25)
L1	675 \pm 219
L2	923 \pm 167
L3	1116 \pm 197
L4	1382 \pm 239
L5	1563 \pm 226
L6	1825 \pm 191
L7	1988 \pm 213
L8	2146 \pm 174
L9	2260 \pm 167
L10	2373 \pm 194
L11	2432 \pm 184
L12	2525 \pm 157
L13	2566 \pm 172
L14	2544 \pm 207
L15	2575 \pm 162
L16	2556 \pm 195
L17	2571 \pm 236
L18	2586 \pm 202
L19	2572 \pm 187
L20	2560 \pm 160
L21	2565 \pm 185
L22	2542 \pm 174
L23	2576 \pm 159
L24	2612 \pm 158
L25	2630 \pm 101

Table S2: Wild-type phyllid lengths by plastochron counting away from the apex of 25 gametophores		
Phyllid position counted back from apex	Mean phyllid length in μm \pm standard deviation (n = 25)	Phyllid length as % of longest phyllid \pm standard deviation (n = 25)
P1	119.78 \pm 32.77	4.47 \pm 1.06
P2	240.1 \pm 97.15	8.85 \pm 3.35
P3	524.55 \pm 187.37	19.6 \pm 6.3
P4	1051.64 \pm 224.63	39.64 \pm 8.38
P5	1703.94 \pm 287.95	64.26 \pm 10.92
P6	2276.21 \pm 259.86	85.61 \pm 7.41
P7	2486.85 \pm 187.95	93.61 \pm 4.08
P8	2506.38 \pm 181.53	94.36 \pm 4.21
P9	2509.71 \pm 205.9	94.39 \pm 3.43
P10	2529.92 \pm 198.94	95.17 \pm 3.37
P11	2509.75 \pm 177.45	94.53 \pm 4.73
P12	2526.86 \pm 197.87	95.05 \pm 3.58
P13	2496.93 \pm 229.53	93.88 \pm 4.74
P14	2490.55 \pm 262.99	93.56 \pm 5.78
P15	2513.99 \pm 288.17	94.29 \pm 6.14

333

334 Table S3

Table S3: Cell shape metrics of phyllids at different positions in heteroblastic series.					
Phyllid position in heteroblastic series	Mean cell numbers in half phyllid \pm standard deviation (n = 5)	Mean cell length in $\mu\text{m} \pm$ standard deviation (n = 5)	Mean cell width in $\mu\text{m} \pm$ standard deviation (n = 5)	Mean cell area in $\mu\text{m}^2 \pm$ standard deviation (n = 5)	Mean cell aspect ratio \pm standard deviation (n = 5)
L3	81 \pm 2	88 \pm 9	25 \pm 1.7	1618 \pm 241	4.3 \pm 0.4
L10	222 \pm 33	95 \pm 6	25 \pm 1.7	1751 \pm 248	4.8 \pm 0.1
L14	311 \pm 45	91 \pm 4	23 \pm 0.5	1597 \pm 126	4.8 \pm 0.2
L16	301 \pm 33	91 \pm 6	23 \pm 0.6	1545 \pm 136	4.9 \pm 0.3
L18	310 \pm 52	91 \pm 5	23 \pm 0.3	1567 \pm 94	4.8 \pm 0.3
L20	326 \pm 28	87 \pm 7	23 \pm 1.0	1479 \pm 123	4.6 \pm 0.4

335

336 Table S4

Table S4: Base Edge and Top cell shape metrics in phyllids sampled from different points of heteroblastic series			
Mean cell area (μm^2) \pm standard deviation per region in each phyllid (n = 5)			
Phyllid	base	edge	top
L3	3037 \pm 449	1961 \pm 135	1266 \pm 104
L10	3355 \pm 211	1516 \pm 104	1265 \pm 585
L14	3343 \pm 138	1671 \pm 265	1168 \pm 844
L16	3349 \pm 236	1619 \pm 195	1099 \pm 956
L18	3230 \pm 289	1596 \pm 185	1134 \pm 429
L20	3055 \pm 158	1516 \pm 234	1114 \pm 462
Mean cell length (μm) \pm standard deviation per region in each leaf in heteroblastic series (n = 5)			
Phyllid	base	edge	top
L3	130 \pm 12	135 \pm 11	74 \pm 3
L10	131 \pm 16	140 \pm 9	74 \pm 2
L14	135 \pm 58	143 \pm 7	72 \pm 3
L16	133 \pm 37	140 \pm 7	71 \pm 4
L18	132 \pm 11	139 \pm 12	72 \pm 3
L20	124 \pm 46	135 \pm 10	70 \pm 4
Mean cell width (μm) \pm standard deviation per region in each leaf in heteroblastic series (n = 5)			
Phyllid	base	edge	top
L3	31 \pm 0.1	22 \pm 0.2	23 \pm 0.1
L10	34 \pm 0.5	17 \pm 0.7	23 \pm 0.1
L14	33 \pm 0.7	17 \pm 0.6	22 \pm 0.3
L16	34 \pm 2.0	17 \pm 1.0	21 \pm 0.5
L18	33 \pm 0.5	17 \pm 0.9	21 \pm 0.4
L20	34 \pm 0.5	16 \pm 0.8	21 \pm 0.5
Mean cell aspect ratio \pm standard deviation per region in each leaf in heteroblastic series (n = 5)			
Phyllid	base	edge	top
L3	5.0 \pm 0.4	8.1 \pm 0.8	3.7 \pm 0.0
L10	4.5 \pm 0.4	11.7 \pm 1.3	3.7 \pm 0.2
L14	4.7 \pm 0.5	11 \pm 1.5	3.7 \pm 0.2
L16	4.7 \pm 0.4	10.7 \pm 0.6	3.9 \pm 0.3
L18	4.6 \pm 0.4	10.6 \pm 1.1	3.7 \pm 0.2
L20	4.3 \pm 0.3	10.9 \pm 1.2	3.7 \pm 0.2

358

359

360

361 Table S5

Phyllid position in heteroblastic series	Length of phyllids in <i>GH3::GUS</i> line (μm) \pm standard deviation (n = 5)	Length of phyllid in <i>pinA pinB</i> line (μm) \pm standard deviation (n = 5)
L1	811 \pm 186	915 \pm 282
L2	1079 \pm 262	1257 \pm 419
L3	1237 \pm 185	1631 \pm 449
L4	1594 \pm 345	1823 \pm 368
L5	1756 \pm 319	2091 \pm 299
L6	1938 \pm 431	2315 \pm 438
L7	2115 \pm 475	2366 \pm 475
L8	2161 \pm 424	2561 \pm 380
L9	2269 \pm 316	2819 \pm 379
L10	2385 \pm 309	2865 \pm 408
L11	2623 \pm 283	2990 \pm 310
L12	2668 \pm 398	3092 \pm 359
L13	2845 \pm 521	3187 \pm 264
L14	2789 \pm 278	3270 \pm 223
L15	2897 \pm 373	3198 \pm 179
L16	3025 \pm 298	3203 \pm 411
L17	2840 \pm 269	3330 \pm 245
L18	2932 \pm 178	3423 \pm 530
L19	3010 \pm 203	3107 \pm 289
L20	3052 \pm 252	3275 \pm 190
L21	3047 \pm 314	3297 \pm 339
L22	2955 \pm 135	3444 \pm 237
L23	2912 \pm 270	3383 \pm 213
L24	3042 \pm 191	3428 \pm 326
L25	2996 \pm 140	3335 \pm 280
L26	3016 \pm 174	3466 \pm 323
L27	3049 \pm 93	3214 \pm 553
L28	2974 \pm 197	3397 \pm 499
L29	2983 \pm 174	3461 \pm 477

362

363 Table S6

Plant	Number of cells per half phyllid	Mean cell area (μm^2) \pm standard deviation	Mean cell length (μm) \pm standard deviation	Mean cell width (μm) \pm standard deviation	Mean cell aspect ratio \pm standard deviation
<i>GH3::GUS a</i>	310	1795 \pm 1238	104 \pm 43	22.8 \pm 7.5	4.9 \pm 2.6
<i>GH3::GUS b</i>	296	1677 \pm 976	99 \pm 35	22.6 \pm 5.9	4.6 \pm 2.0
<i>GH3::GUS c</i>	310	1360 \pm 796	95 \pm 38	19.6 \pm 5.4	5.3 \pm 3.1
<i>GH3::GUS d</i>	278	1728 \pm 1199	101 \pm 39	21.6 \pm 7.2	4.9 \pm 2.1
<i>GH3::GUS e</i>	287	1528 \pm 986	96 \pm 41	21.4 \pm 6.3	4.8 \pm 2.7
<i>pinA pinB a</i>	193	1922 \pm 1050	127 \pm 50	21.4 \pm 7.5	6.3 \pm 2.7
<i>pinA pinB b</i>	164	2287 \pm 1522	127 \pm 45	23.9 \pm 8.6	5.6 \pm 2.2
<i>pinA pinB c</i>	196	1972 \pm 1488	117 \pm 44	22.5 \pm 7.9	5.4 \pm 2.0
<i>pinA pinB d</i>	155	1968 \pm 989	127 \pm 44	21.8 \pm 6.0	6.2 \pm 2.5
<i>pinA pinB e</i>	235	1586 \pm 930	117 \pm 46	19.0 \pm 5.3	6.3 \pm 2.6

364

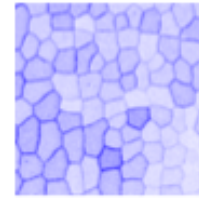
365 Table S7

Table S7: Quantitative comparison of <i>GH3::GUS</i> to <i>pinA pinB</i> mutants						
Region and background		Mean number of cells ± standard deviation (n phyllids = 5)	Mean cell area (μm^2) ± standard deviation	Mean cell length (μm) ± standard deviation	Mean cell width (μm) ± standard deviation	Cell Aspect Ratio ± standard deviation
Top	<i>GH3::GUS</i>	227 ± 12	1247 ± 82	82 ± 2.6	20 ± 0.9	4.1 ± 0.1
	<i>pinA pinB</i>	116 ± 32	1362 ± 81	95 ± 2.0	20 ± 0.9	5.0 ± 0.2
Edge	<i>GH3::GUS</i>	36 ± 7	1787 ± 138	161 ± 9.4	17 ± 0.8	10 ± 0.9
	<i>pinA pinB</i>	44 ± 11	2028 ± 104	169 ± 5.3	19 ± 0.7	9.3 ± 0.5
Base	<i>GH3::GUS</i>	33 ± 12	3941 ± 213	151 ± 3.7	35 ± 1.4	4.5 ± 0.1
	<i>pinA pinB</i>	29 ± 10	4034 ± 403	164 ± 14	34 ± 1.8	4.9 ± 0.5

Moss phyllid cell segmentation protocol

1. Toluidine blue staining phyllids:

- i. Remove phyllid from desired position in heteroblastic series.
- ii. Clear in Hoyer's medium overnight (Anderson, 1954).
- iii. Wash tissue with deionised water at least three times.
- iv. Place tissue in 2M NaOH for 2 hours.
- v. Wash tissue with deionised water at least three times.
- vi. Stain with 0.05% Toluidine Blue for two minutes.
- vii. Destain for 10 minutes in water.
- viii. Wash two or more times with DI water and leave until ready to mount.



Region of toluidine blue stained phyllid.

2. Image capture

- i. Capture images with a maximum pixel resolution of 1024 in the longest dimension using a 20 x objective.
- ii. Save images of the same phyllid with sequential tags e.g. Myname_Treatment_shoot01_Leaf20_img0001.tif
- iii. Ensure there is >25% overlap between fields of view in each image.

3. Image stitching (see supporting illustrations below)

- i. Open Fiji.
- ii. Open an image selected to represent a series.
- iii. Select from "Plugins" >> "Segmentation" >> "Trainable Segmentation".
- iv. Use tools on the FIJI task bar to **pan around your image** and **zoom in and out** in the "Trainable Segmentation" window.
- v. Use the **freehand drawing tool** to draw along some of the cell walls, on the image in the "Trainable Segmentation" window.
- vi. When a set of cell walls is highlighted (marked by a yellow line), click "Add to class 2" (the line will turn green) and repeat this step a few times.
- vii. Then mark a non-cell wall area i.e. within a cell or outside of the phyllid, and click "Add to class1".
- viii. Click the Train classifier tool.
- ix. If you are happy with the result (I am in this instance), then click the button "Save data".
- x. Save the data in a new file named "trainingdata".
- xi. Click the button "Create result" to generate a black and white (binary) image of the result.
- xii. Save the image "classification result" (with a more appropriate name) e.g., TS_Original_name_of_image.tif
- xiii. Complete this segmentation step for all images, saving each one separately.
- xiv. Move all images from a single phyllid to a single folder.
- xv. Stitch the images together using Plugins >> Stitching >> Deprecate >> Stitch directory with images (unknown arrangement).
- xvi. Click "Browse" from the pop up box and select a folder where the images for one phyllid are saved.
- xvii. Click OK
- xviii. If there are stitching problems, try stitching fewer images at once and later putting part stitched images together.
- xix. Save the image.

4. Manual refinement of stitched images using GIMP (see supporting illustrations below)

- i. Open GIMP.
- ii. Open the stitched image from step 3.
- iii. Save the image with a GIMP (.xcf) extension.
- iv. Select the whole image, and copy and paste.
- v. Click "new layer" twice, and create a transparent layer.
- vi. Select the new layer using the layers panel.
- vii. Select the paint bucket icon from the tools panel, and fill the new layer in black by clicking anywhere on the picture.
- viii. Move the new layer below the pasted layer.
- ix. Select the pasted layer from the layers panel.
- x. Then select "Colors" >> "Threshold" and click "OK" to turn the image to black and white.
- xi. Select the pencil button from the tools layer and adjust the size and brush to a similar width to wall widths.
- xii. Trace a black line just to side of the midrib. Maintain a continuous line of white the length of the midrib to the left of the midrib. By holding the shift key as you click you will see a line which will be traced by the pencil tool and become black.
- xiii. Once you have drawn a black line through the centre on the phyllid entirely separating the two sides, change the colour of the pencil tool to white and look for cell walls that are not complete and join them (if unsure compare with original microscope image). Only do this for one side of the phyllid.
- xiv. If cell walls appear fused, change the pencil tool to black and fill cells to ensure they have continuous black centre.
- xv. Select the "fuzzy select tool".
- xvi. Click on the white of the image to select a contiguous area comprising the cell wall outlines of a half phyllid (if both sides are selected the black line through the midrib was incomplete).
- xvii. Hold "Ctrl" and press "I" to invert the previous selection.
- xviii. "Delete" the speckles that are not connected to cell walls to leave a segmented half-phyllid.
- xix. "Flatten" the image and save it as a .tif file.
- xx. Open the .tif file "Gimp_edited_stitched_phyllid_01.tif" in Fiji.
- xxi. Select "Process">> "Smooth" and smooth three times.
- xxii. Convert the image to binary mode (select "Process" >> "Binary" >> "Make Binary").
- xxiii. Select "Plugins" >> "Skeleton" >> "Skeletonize(2D/3D)".
- xxiv. Select "Process">> "Smooth" and smooth three times.
- xxv. Convert the image to binary mode again and save it as a new .tif file ("Skeleton_edited_phyllid_01.tif").
- xxvi. Touch up traces by referring to original microscope image using the pencil tool and bucket fill tools in GIMP or in FIJI.
- xxvii. Skeletonize, smooth, and make binary the image as above and and save it as a new .tif file "Finished_phyllid_01.tif"

5. Cell size/shape analysis (see supporting illustrations below)

- i. Open the "Finished_phyllid" file in Fiji.
- ii. To set the scale, select "Analyze" >> "Set Scale".
- iii. To scale later images in a series to the first image, "Click to remove scale" and tick the box "Global".

- iv. Calculate the scale by opening an image with a measured scale bar in it. Select the "Straight" free hand line tool and draw a line across the length of the scale bar.
- v. Select the "Analyze" >> "Set Scale" tool and type the length of the scale bar into the "Known distance" box. Fiji automatically calculates the conversion ratio of pixels to units for you.
- vi. Select the measurements you want to make using select "Analyze" >> "Set measurements".
- vii. Select areas of the image to be measured using "image" >> "adjust" >> "threshold", and slide the threshold scale so that the whole image turns red.
- viii. Select "Analyze" >> "Analyze Particles".
- ix. Tick the boxes "Exclude on edges", "Display results" and "Add to manager".
- x. Save the results from the "Results" window by selecting "File" >> "Save As" e.g. "Cell_data_Phyllid01.csv".
- xi. Use data for variable comparison in other packages

6. Phyllid size analyzes (see supporting illustrations below)

- i. Open the "Finished_phyllid" file in Fiji.
- ii. Set the scale as described in Section 5.
- iii. Select areas of the image to be measured using "image" >> "adjust" >> "threshold", and slide the threshold scale so that only the cell walls are outlined in red.
- iv. Set the "Analyze particles" option to "include holes option".
- v. Select the "Straight" line drawing tool and then select "Segmented line".
- vi. Extend the line by clicking along the length of the phyllid outline and when finished right click.
- vii. Select the "Analyze" >> "Measure" option to return the length of the line you just drew.
- viii. Save this new results window, "File" >> "Save As" (ie. Whole_Leaf_measurements_Leaf01.csv).
- ix. Use data for variable comparison in other packages

3. Image stitching

3ii.



3iii.



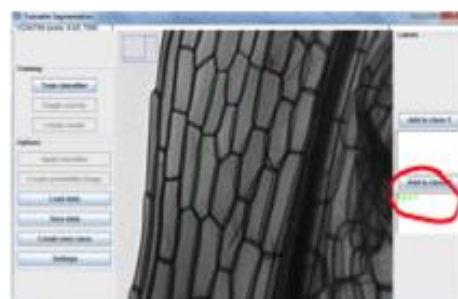
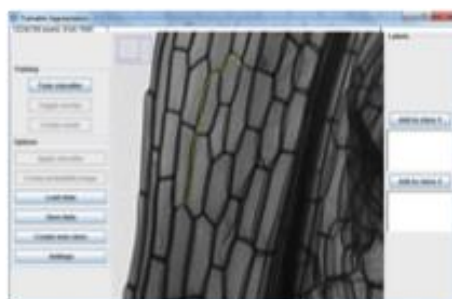
3iv.



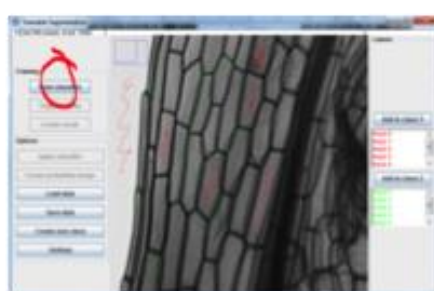
3v.



3vi.



3vii.



3viii.



4. Manual refinement of images

4v.



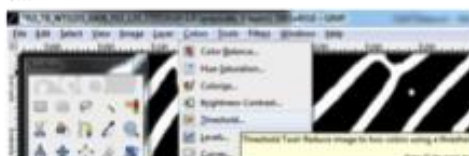
4vii.



4viii.



4x.



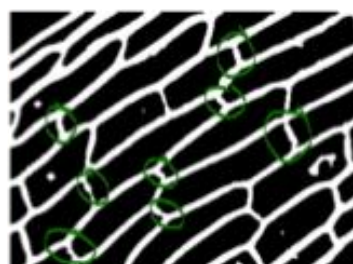
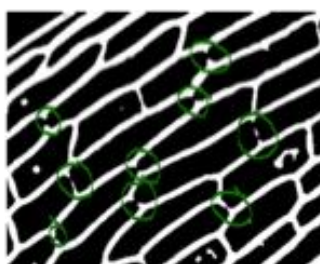
4xi.



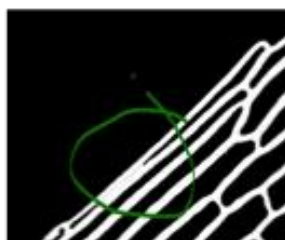
4xii.



4xiii.



4xiv.



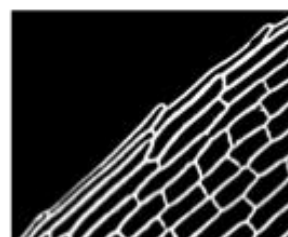
4xv.



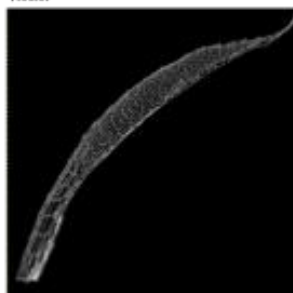
4xvi.



4xviii.



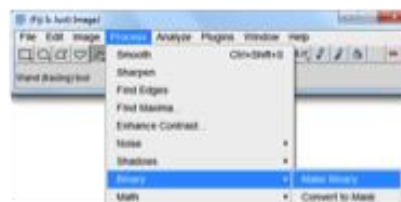
4xix.



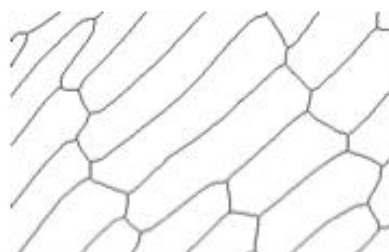
4xxi.



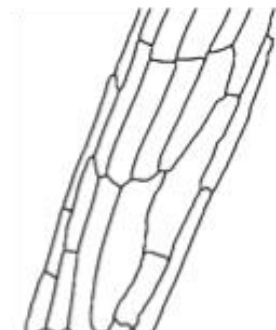
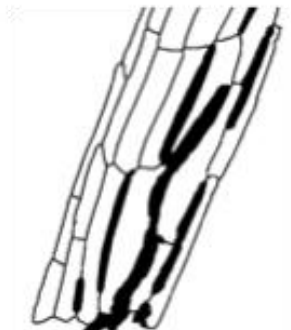
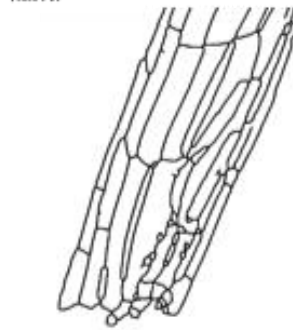
4xxii.



4xxii.



4xxvi.

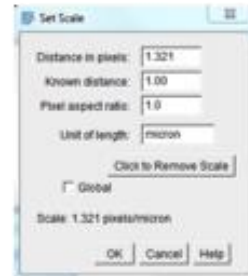


5. Cell size and shape analyzes

5iii.



5iii.



5iv.



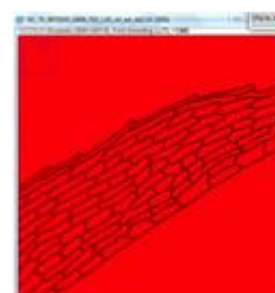
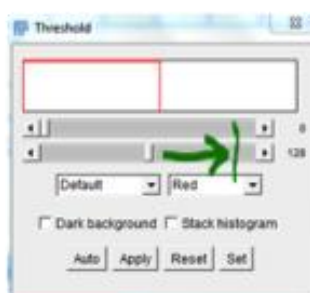
5v.



5vi.



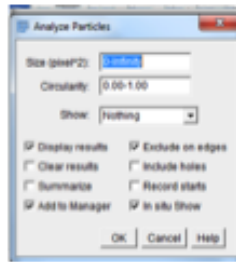
5vii.



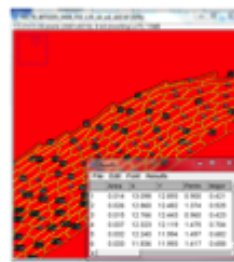
5viii.



5ix.

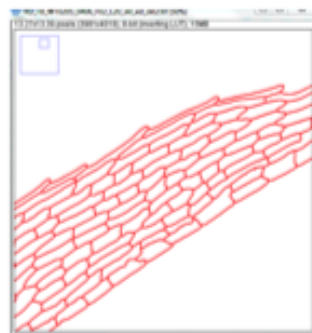


5x.



6. Phyllid size analyzes

6iii.



6v.

